JOURNAL OF GEOPHYSICAL RESEARCH, VOL. 113, A04308, doi:10.1029/2007JA012910, 2008

The influence of magnetospheric substorms on SuperDARN radar backscatter

J. A. Wild[1] and A. Grocott[2]

Received 24 October 2007; revised 3 January 2008; accepted 5 February 2008; published 25 April 2008.

[1] The SuperDARN ionospheric radar network is a leading tool for investigating the near-Earth space environment. However, reductions in ionospheric backscatter have been reported during magnetospheric substorms. We have therefore investigated the impact of substorms upon SuperDARN backscatter during 3005 substorms and find that the global level of scatter maximizes just prior to substorm onset. In the nightside ionosphere, backscatter poleward of ~70° magnetic latitude is reduced, with radar echoes shifting to lower latitudes. An examination into the frequency-dependence of nightside backscatter evolution during substorms reveals that although most backscatter data is based upon operations in the 08–14 MHz range, higher operating frequencies may offer improved performance in the period just prior to and immediately following expansion phase onset. We suggest that the SuperDARN array of high-frequency coherent-scatter radars, and in particular those radars with the ability to simultaneously operate at dual frequencies, will play a key role in future space- and ground-based studies of substorms.

Citation: Wild, J. A., and A. Grocott (2008), The influence of magnetospheric substorms on SuperDARN radar backscatter, *J. Geophys. Res.*, *113*, A04308, doi:10.1029/2007JA012910.

1. Introduction

[2] Since the concept was first proposed by *Akasofu* [1964], the substorm has proven to be one of the greatest challenges in solar-terrestrial physics. Despite advances in the field, the timing, location and possible triggering mechanism of substorm onset remains unclear, with competing models seeking to explain the instability underlying the explosive reconfiguration during the substorm expansion phase [e.g., *Lui*, 2003].

[3] The Super Dual Auroral Radar Network (SuperDARN: *Chisham et al.* [2007]) is an international array of 18 high-frequency (HF) coherent-scatter ionospheric radars with fields-of-view covering a significant fraction of the auroral and polar ionosphere in both the northern and southern hemispheres. Data from a subset of the network can be analyzed to provide detailed localized measurements of ionospheric plasma dynamics while measurements from all radars may be combined using the "potential mapping" technique of *Ruohoniemi and Baker* [1998] in order to estimate the global ionospheric convection pattern in both hemispheres. Consequently, SuperDARN has become one of the pre-eminent ground-based tools for the investigation of the space and ionospheric plasma environment and a vital tool when undertaking combined space- and ground-based investigations [e.g., *Amm et al.*, 2005].

[4] The SuperDARN system has provided significant inroads to the substorm problem by revealing ionospheric flows in the nightside ionosphere during both the growth and expansion phase, the response of the ionospheric convection pattern to the increased tail reconnection rate during the expansion phase and the family of substorm-associated convection transients observable in the nightside ionosphere (the reader is directed to *Chisham et al.* [2007, section 5], for a comprehensive review). However, an equatorward migration of radar backscatter has previously been reported during the substorm growth phase [*Lewis et al.*, 1997] while a loss of backscatter (upon which all SuperDARN data products depend) is sometimes reported in the nightside ionosphere during substorm onset, an effect attributed to absorption of HF radio waves by the enhanced electron densities in the substorm precipitation region [*Milan et al.*, 1999] and rapid changes in HF propagation conditions [*Gauld et al.*, 2002].

[5] Apart from case-studies of individual substorms, the only previous study to examine the impact of magnetospheric substorms upon SuperDARN radar backscatter was that of *Provan et al.* [2004]. In that study, SuperDARN data was used to examine the northern hemisphere ionospheric convection pattern during 67 substorms identified by the far ultra violet (FUV) auroral imager on board the IMAGE satellite. Provan and coworkers reported little change in the occurrence of radar backscatter during the substorm growth phase with the highest number of radar echoes observed in the post-noon sector dayside ionosphere. Following substorm onset, this post-noon sector backscatter grew stronger while nightside scatter diminished and showed some evidence of equatorward migration.

[1]Department of Communication Systems, Lancaster University, Lancaster, UK.
[2]Department of Physics and Astronomy, University of Leicester, Leicester, UK.

0148-0227/08/2007JA012910$09.00

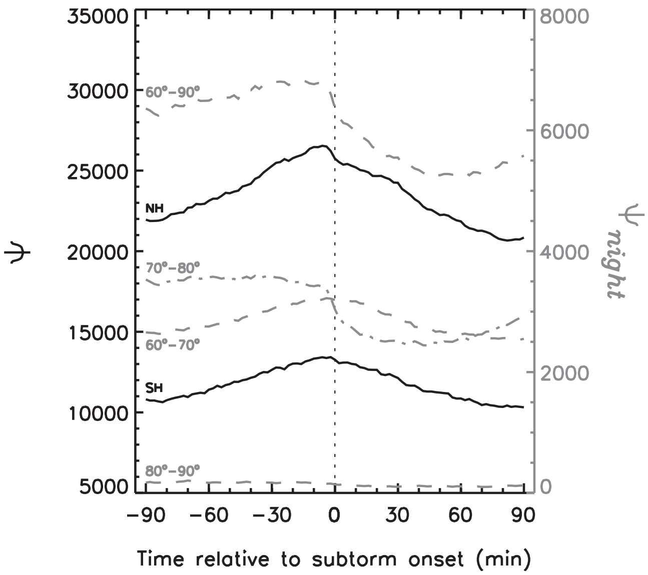

Figure 1. Variations in the backscatter parameter Ψ presented as a function of time relative to substorm onset. The solid traces labeled "NH" and "SH" show backscatter variations in the northern and southern hemispheres, respectively, according to the left-hand vertical axis. The dashed traces indicate backscatter variations in the nightside ionosphere (Ψ_{night}) in both hemispheres between 21–03 MLT. Latitudinal ranges covering 60°–70°, 70°–80° (dot-dashed), 80°–90° and 60°–90° are indicated and correspond to the right-hand vertical axis.

[6] Given the increasing use of SuperDARN measurements for both global and localized investigations of ionospheric flow during substorms and the upcoming focus of international research effort on the substorm process prompted by NASA's Time History of Events and Macroscale Interactions during Substorms (THEMIS) mission, a comprehensive investigation into the influence of magnetospheric substorms upon the level of ionospheric backscatter recorded by the SuperDARN network is desirable. Such a study is presented below.

2. Methodology

[7] In order to examine SuperDARN backscatter statistics during substorms, it is first necessary to identify a set of candidate events. *Frey et al.* [2004] analyzed auroral observations made by the IMAGE FUV instrument between May 2000 and December 2002, identifying 2437 individual substorms. This list of events, subsequently extended to December 2005 and including 4193 substorms, forms the basis of the present study. Of these events, we have excluded those substorms that are known to have occurred within ±2 h of another substorm. While we cannot exclude substorms that occurred within 2 h of an earlier/later event not observed by IMAGE FUV (e.g., due to unfavorable orbital position), this measure will reduce the impact of multiple substorm onsets/intensifications upon our analysis. Consequently, the list of substorms to be examined is reduced to 3005 individual events from May 2000 to December 2005. Intervals of data spanning the period ±90 min from each of the expansion phase onsets listed by *Frey et al.* [2004] have been assessed.

[8] The field-of-view (f-o-v) of each SuperDARN radar comprises 16 beams separated by ~3.24° in azimuth and with each beam subdivided in 75 range gates. During standard operation, each range gate is 45 km in length with the first range gate beginning 180 km from the radar site. Typically, the dwell time for each beam is either 3 or 7 s, giving a full 16-beam scan, covering 52° in azimuth and over 3000 km in range (an area of over 3×10^6 km^2) every 60 or 120 s. However, each radar can operate in non-standard sounding modes with the number of beams, length of range gate, distance to first range, scan pattern, dwell time and operating frequency being fully adjustable. As such, data from individual SuperDARN radars have been mapped into the spatial grid utilized by the map potential analysis technique of *Ruohoniemi and Baker* [1998]. This global grid system has grid cells which span 1° in magnetic latitude (~111 km projected onto the Earth's surface), and ~111 km in the longitudinal dimension. This gridding system approximately equalizes cell areas, whereas the more conventional choice of a grid defined by fixed steps in latitude and longitude suffers from severe variations in cell area at differing latitudes. This technique is also the same at that used previously by *Provan et al.* [2004].

[9] In the present study, backscatter data from all available radars are gridded (without spatial or temporal averaging) at 2 min cadence. Only echoes determined to originate from ionospheric sources are included, with ground-scatter echoes being rejected at this stage. The number of gridded data points is then assessed for the 2 min interval in question. The quantity of observed backscatter in the grid is then weighted to take into account the number of radars operating at that time in order to produce a backscatter parameter Ψ, given by:

$$\Psi(t) = \frac{n_{scatter}(t)}{n_{radar}(t)} \tag{1}$$

where $\Psi(t)$ is the backscatter parameter, $n_{scatter}(t)$ the number of backscatter measurements and n_{radar} the number of operating radars, all measured at time t. By weighting Ψ in this way, variations in the number of operating radars over the 2000–2005 epoch under investigation will be minimized.

[10] We note that by gridding data according to a geomagnetic coordinate system, variations in the location of substorm expansion phase onset (as described by *Frey et al.* [2004]) imply that the results will provide a insight into the backscatter response relative to the statistically averaged substorm onset location. Nevertheless, this will allow the results to be compared with other statistically well-defined features such as the auroral oval and the ionospheric projection of the magnetospheric cusp.

3. Results

[11] Figure 1 presents the variation in Ψ summed over the 3005 substorms described above as a function of time relative to substorm expansion phase onset. In this case, Ψ has first been computed for all northern hemisphere radars, and then for all southern hemisphere radars (solid traces

labeled "NH" and "SH" respectively) with the denominator in equation (1) being replaced by the number of northern/southern hemisphere radars available as appropriate. Clearly, the backscatter recorded by both northern and southern hemisphere SuperDARN radars during the 90 min prior to substorm onset gradually builds, peaking 5–10 min prior to substorm onset before falling to the pre-substorm level by 90 min after onset. In the northern hemisphere, the level of backscatter observed at $t + 90$ min is slightly lower than that at $t - 90$ min, but shows evidence of recovery toward the pre-substorm level.

[12] The weighting of the Ψ parameter takes into account the fact that fewer SuperDARN radars were operating in the southern hemisphere compared to the northern hemisphere during the 2000–2005 interval under investigation. It is therefore interesting to note that the northern hemisphere backscatter parameter is typically twice that in the southern hemisphere. Although the SuperDARN radars used are virtually identical and all located within a few degrees of 60° magnetic latitude, it is possible that this systematic difference in the amount of backscatter is an instrumental effect. Interhemispheric differences in the HF radio propagation conditions within radar fields-of-view may also be responsible. For example, northern hemisphere radars observe a considerable number of echoes from so-called "one-and-a-half-hop" scatter; ionospheric radar backscattered that is reflected by the ground/sea before propagating through an ionospheric path to the receiver. The increased abundance of one-and-a-half-hop scatter in the northern hemisphere (where the radars typically overlook ground or sea) compared to the southern hemisphere (where the radars mainly overlook the generally icy Antarctic continent) may explain this interhemispheric difference.

[13] The traces labeled "NH" and "SH" include data at all latitudes and local times. As such, they show the "global" variation in backscatter. However, it is reasonable to expect the largest impact of substorms on radar backscatter will occur in the nightside ionosphere. Thus the broken lines in Figure 1 present the variations of Ψ when only scatter observed between 21–03 MLT (northern and southern hemispheres combined) is included in the numerator of equation (1). Here, Ψ is further broken down to indicate the variation in backscatter in the 60°–70°, 70°–80°, 80°–90° and 60°–90° magnetic latitude ranges. In the 60°–70° range, the variation in backscatter resembles the global trend, rising from $t = -90$ min to peak within a few minutes of substorm onset (in this case just after onset) and then gradually falling to pre-substorm levels. The 70°–80° range is hardest hit, with the level of backscatter dropping by ~30% within a few minutes of onset. Very little backscatter is observed within the polar cap (mlat $\geq$ 80°), but the level is approximately constant throughout the substorm period.

[14] Figure 2 shows changes in the spatial distribution of Ψ in the crucial period from 18 min prior to the substorm expansion phase ($t - 18$ min) to 18 min after onset ($t + 18$ min). The distribution of Ψ in both the northern and southern hemispheres from $t - 18$ to $t + 18$ to min is presented in the magnetic latitude/magnetic local time coordinate system shown in the key. In order to improve the statistical significance of the data, the grid size in both the meridional and zonal directions has been doubled (i.e., 2° in magnetic latitude and ~220 km in the longitudinal dimension). The change in backscatter ($\Delta\Psi$) in both hemispheres is presented in the same coordinate system at 6 min time steps. In each case, $\Delta\Psi$ is computed relative to the backscatter distribution at the time of the previous plot (and only where Ψ is greater than 10). The values of Ψ and $\Delta\Psi$ are color-coded according to the appropriate color bar.

[15] At $t - 18$ min, the distribution of backscatter roughly corresponds to the expected location of the auroral oval, spanning all local times and found at higher magnetic latitudes in the dayside ionosphere than in the nightside. In the northern hemisphere dayside ionosphere, most scatter is observed in the ~75°–80° magnetic latitude region, distributed somewhat asymmetrically about noon. Backscatter maximizes in the morning (06–12 MLT) sector with a minimum around dusk, somewhat in contrast to the post-noon maximum reported by *Provan et al.* [2004]. Although fewer southern hemisphere data are available (as discussed above), there is evidence that the dayside maximum occurs in the afternoon sector with a minimum in the morning sector. In the nightside ionosphere (both hemispheres), backscatter is greatest in the ~66°–76° magnetic latitude zone and relatively evenly distributed about midnight.

[16] Between $t - 18$ min and $t - 0$ min, the amount of dayside scatter increased slightly, indicated by the orange/red $\Delta\Psi$ color coding in the dayside ionosphere as shown in Figure 2, while the amount of nightside scatter remained broadly steady, consistent with the trends presented in Figure 1. Indeed, the data presented in Figure 1 indicate that the overall scatter in each hemisphere is tending to a maximum as the time of substorm onset approaches, suggesting that the regions where backscatter is increasing more than compensate for those where backscatter is reducing.

[17] At the time of substorm onset ($t - 0$ min), there is a marked reduction in nightside backscatter (indicated by the purple/blue color-coding) in the auroral zone in both hemispheres. In the northern hemisphere, the backscatter reduction is greatest in the ~70°–80° magnetic latitude region between ~19–03 MLT, while in the southern hemisphere there is some evidence that the effect extends from ~21–05 MLT (albeit based upon fewer data points). Meanwhile, in the northern hemisphere, where there are more backscatter data at lower latitudes, the level of backscatter in the region equatorward of ~65° increases significantly at substorm onset, suggesting that the scatter has shifted in location. This displacement of backscatter to lower latitudes occurs across most local times from dusk to dawn.

[18] The reduction in nightside backscatter in the ~70°–80° magnetic latitude region continues over the next 18 min (lower 3 rows presented in Figure 2). At $t + 6$ min, the region in which northern hemisphere scatter is falling most rapidly appears to move from the pre- to post-midnight sector. A similar motion is observed in the southern hemisphere at $t + 12$ min. Also, the lower latitude region of increased scatter extends to virtually all local times in the northern hemisphere at $t + 6$ min. We note that throughout the interval presented, backscatter in the polar cap is broadly unchanged (as indicated in Figure 1).

[19] Figure 3 shows relative backscatter parameter variations in the nightside ionosphere (21–03 MLT, between (a) 60°–70° and (b) 70°–80° magnetic latitude) sorted by

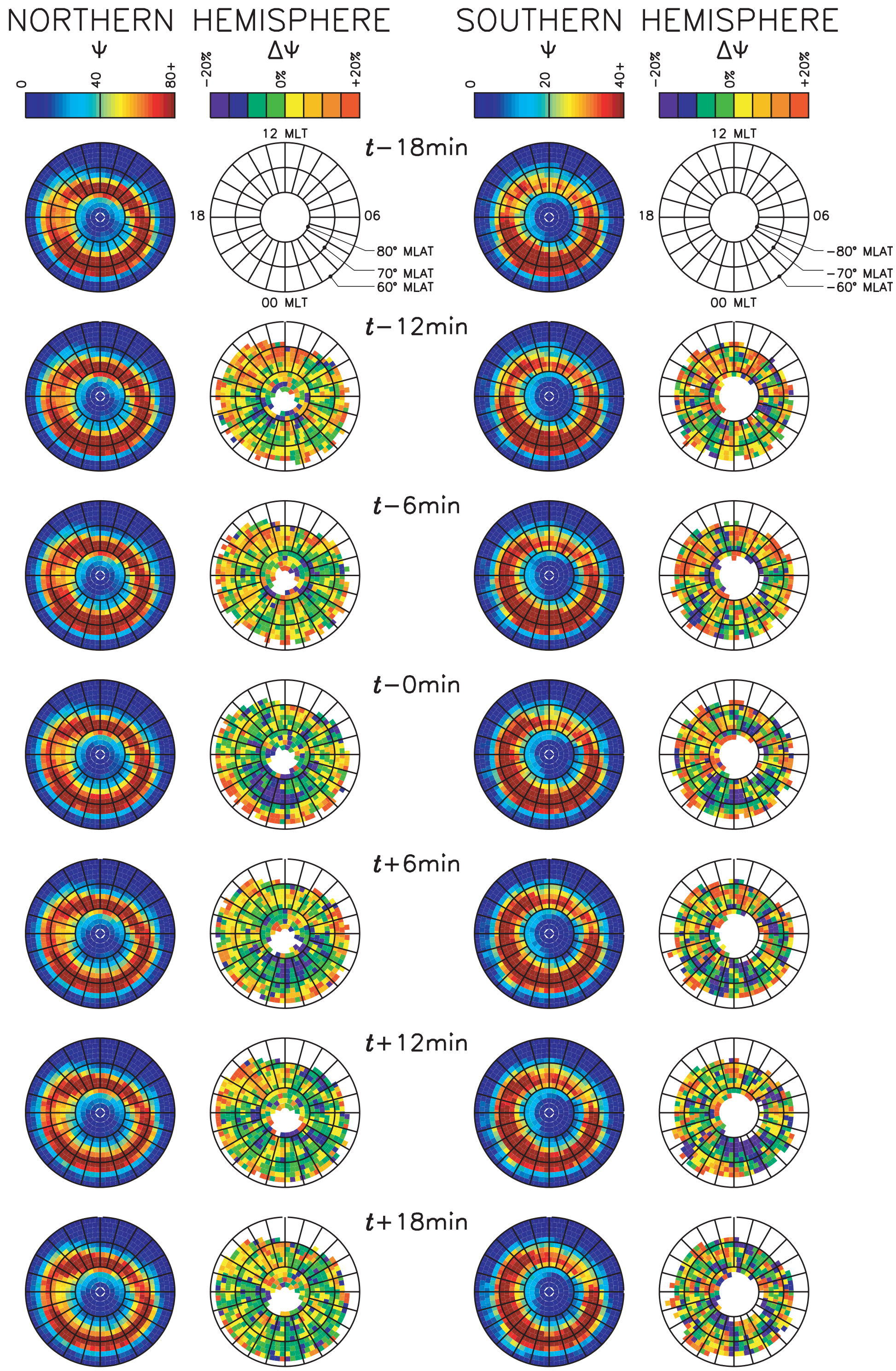

Figure 2. The spatial variation in backscatter parameter (Ψ) around substorm expansion phase onset.

radar operating frequency (Ψ_{freq}). This is computed by substituting $n_{radar}(t)$ in equation (1) by the number of radars operating at a given frequency, $n_{radar}(t, \nu)$. Thus the Ψ_{freq} backscatter parameter is weighted according to the number of radars operating at the selected frequency. The baseline value is simply the mean value of the Ψ_{freq} computed in each frequency band during the $t - 90$ to $t - 60$ min interval and reflects the average pre-onset level of the backscatter parameter. $\Sigma\Psi_{freq}$ is the sum of Ψ_{freq} in each frequency band computed over the entire epoch and is therefore related to the total number of backscatter measurements made in that band.

[20] In the 60°–70° magnetic latitude region (Figure 3a), the variations in backscatter parameter follow the broad trend presented in Figure 1 (i.e., increasing prior to substorm onset and falling afterward). However, there are

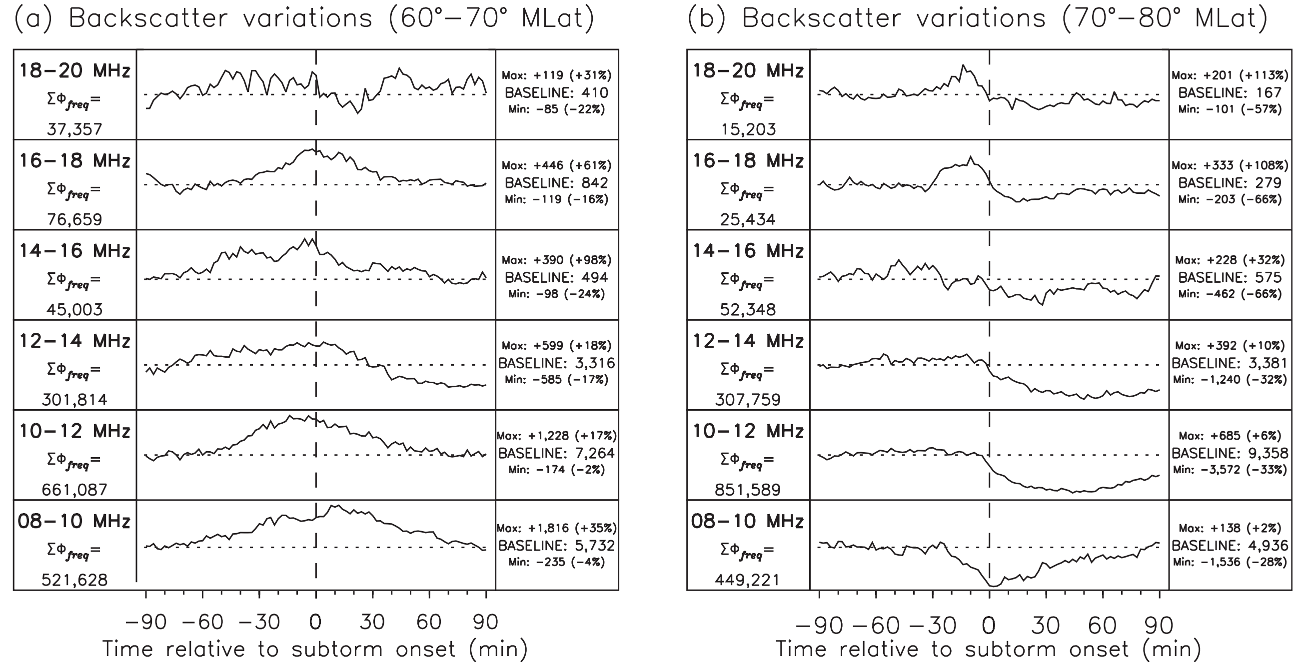

Figure 3. Variation of the frequency-dependent backscatter parameter Ψ_{freq} in the nightside region between (a) 60°–70° and (b) 70°–80° magnetic latitude, as a function of time relative to substorm onset. Each panel shows the variations about the baseline level of Ψ_{freq} for the state frequency range.

subtle differences in the backscatter variations at each operating frequency. If we consider that of the 4193 substorms in the *Frey et al.* [2004] list, 85% occurred in the 60°–70° region, then these differences may have important consequences for the operation of the SuperDARN radars when studying substorms. SuperDARN radars most commonly observed echoes in the 8–14 MHz range (as indicated by the large baseline values and $\Sigma\Psi_{freq}$ in these frequency bands). Clearly, this is due to these being the preferred operating frequencies (since backscatter cannot be observed in a frequency band that the radar is not sounding). Operations in the 14–18 MHz range are less common, with operation in the 18–20 MHz range being somewhat unusual (with consequently poor backscatter statistics). However, we note that in the 12–14 MHz range, despite reasonable overall performance, the backscatter parameter drops below the pre-growth phase baseline level ~30 min after substorm onset. In contrast, in the 8–10 MHz range, backscatter continues to increase for ~10 min following substorm onset and does not fall to the baseline level until t + 90 min.

[21] In the 70°–80° magnetic latitude range (Figure 3b), the backscatter parameter profile is very different. Radar measurements in the 8–14 MHz range account for the majority of the backscatter indicated in the 70°–80° nightside profile presented in Figure 1. However, in the 8–10 MHz range, we note that the backscatter minimizes at the time of substorm onset, having begun to fall from the baseline level at t − 30 min. In the 10–14 MHz range, backscatter is roughly constant until the time of substorm onset (slightly before substorm onset in the case of 10–12 MHz) but then falls steadily over the first ~30 min of the expansion phase. At higher frequencies, the backscatter trend is quite different. For example, in the 16–18 MHz band, although there is significantly less scatter overall (in part because these frequencies are utilized less often), there is a notable increase in the level of backscatter during the ~30 min prior to onset. Indeed, in the frequency bands above 14 MHz, there is only a modest fractional reduction in backscatter in the crucial ~5 min after onset (albeit imposed on a lower level of pre-onset scatter compared to lower operating frequencies).

4. Conclusions

[22] We have performed an analysis of SuperDARN radar backscatter during 3005 substorms identified from IMAGE FUV observations in the period May 2000 to December 2005. We find that the global level of backscattered signal rises during the 90 min preceding substorm onset by ~20%, peaking a few minutes prior to the expansion phase and then gradually declining to approximately the pre-substorm level over the following 90 min. In the nightside ionosphere, the level of backscatter begins to fall a few minutes prior to substorm onset, with an overall reduction of ~25% in the hour following onset. This modest "loss" of backscatter is concentrated in the region poleward of ~70° magnetic latitude, with significant levels of backscatter actually shifting to lower magnetic latitudes. Although radar operations in the 8–14 MHz frequency range in the nightside ionosphere generally result in a significant fraction of backscatter data, there is evidence that operations at frequencies outside this range might prove advantageous. For example, the 8–10 MHz band, which yields excellent radar backscatter in the 60°–70° magnetic latitude region of the nightside ionosphere does not perform as well in the 70°–80° region within ±30 min of substorm onset.

[23] The upgrade of a subset of the SuperDARN radars to provide a "stereo" capability has enabled simultaneous

sounding at two different frequencies [*Lester et al.*, 2004]. We therefore propose an evaluation of dual frequency operations in the nightside ionosphere during substorms, simultaneously sounding in the 8–14 and 14–20 MHz bands in order both to maximize the overall level of backscatter and provide an uninterrupted diagnostic capability (albeit with less backscatter) in the ionospheric regions associated with substorm expansion phase onset.

[24] NASA's THEMIS mission [*Frey et al.*, 2004] launched in February 2007, is specifically designed to address the present uncertainty in the location and timing of substorm expansion phase onset in the Earth's magnetic tail. The mission comprises five identically instrumented probes with orbits arranged such that during key observing seasons, the spacecraft align radially every four days in order to measure the timing and evolution of the signatures of substorm onset. Crucial to achieving this aim is a complementary network of ground-based experiments, including a dedicated array of all-sky imagers and fluxgate magnetometers [*Donovan et al.*, 2006]. Given the upcoming focus upon the substorm problem as a result of the THEMIS mission and the huge potential contribution to be made by the SuperDARN radar network, the possible benefits of dual-frequency operations to SuperDARN radar performance during the substorm expansion phase may prove to be crucial.

[25] **Acknowledgments.** The authors are grateful to H. U. Frey (Univ. of California, Berkeley) for making the list of substorms available to the community and to M. Lester for helpful comments on the manuscript. We are also indebted to the PIs of the various SuperDARN radars, without whose efforts this study would not have been possible. Throughout this study, AG was supported by STFC rolling grant number PP/E000983/1.

[26] Wolfgang Baumjohann thanks Olaf Amm and Gareth Chisham for their assistance in evaluating this paper.

References

Akasofu, S. I. (1964), The development of the auroral substorm, *Planet. Space Sci.*, *12*(4), 273–282.

Amm, O., et al. (2005), Coordinated studies of the Geospace environment using Cluster, satellite and ground-based data: An interim review, *Ann. Geophys.*, *23*, 2129–2170.

Chisham, G., et al. (2007), A decade of the Super Dual Auroral Radar Network (SuperDARN): Scientific achievements, new techniques and future directions, *Surv. Geophys.*, *28*, 33–109, doi:10.1007/s10712-007-9017-8.

Donovan, E., et al. (2006), The THEMIS all-sky imaging array - System design and initial results from the prototype imager, *J. Atmos. Sol. Terr. Phys.*, *68*(13), 1472–1487, doi:10.1016/j.jastp.2005.03.027.

Frey, H. U., S. B. Mende, V. Angelopoulos, and E. F. Donovan (2004), Substorm onset observations by IMAGE-FUV, *J. Geophys. Res.*, *109*, A10304, doi:10.1029/2004JA010607.

Gauld, J. K., T. K. Yeoman, J. A. Davies, S. E. Milan, and F. Honary (2002), SuperDARN radar HF propagation and absorption response to the substorm expansion phase, *Ann. Geophys.*, *20*, 1631–1645.

Lester, M., et al. (2004), Stereo CUTLASS - A new capability for the SuperDARN HF radars, *Ann. Geophys.*, *22*, 459–473.

Lewis, R. V., M. P. Freeman, A. S. Rodger, G. D. Reeves, and D. K. Milling (1997), The electric field response to the growth phase and expansion phase onset of a small substorm, *Ann. Geophys.*, *15*, 289–299.

Lui, A. T. Y. (2003), Cause of magnetospheric substorms, *Plasma Phys. Controlled Fusion*, *45*(6), 841–852.

Milan, S. E., J. A. Davies, and M. Lester (1999), Coherent HF radar backscatter characteristics associated with auroral forms identified by incoherent radar techniques: A comparison of CUTLASS and EISCAT observations, *J. Geophys. Res.*, *104*(A10), 22,591–22,604.

Provan, G., M. Lester, and S. B. M. S. E. Milan (2004), Statistical study of high-latitude plasma flow during magnetospheric substorms, *Ann. Geophys.*, *22*, 3607–3624.

Ruohoniemi, J. M., and K. B. Baker (1998), Large-scale imaging of high-latitude convection with Super Dual Auroral Radar Network HF radar observations, *J. Geophys. Res.*, *103*(A9), 20,797–20,811.

A. Grocott, Department of Physics and Astronomy, University of Leicester, University Road, Leicester, LE1 7RH, UK.

J. A. Wild, Department of Communication Systems, InfoLab 21, Lancaster University, Lancaster, LA1 4WA, UK. (j.wild@lancaster.ac.uk)